Giant voltage-control-magnetic-anisotropy (VCMA) effect in a crystallographically strained CoFe system

Y. Kato*, H. Yoda, Y. Saito+, S. Oikawa, K. Fujii, M. Yoshiki, K. Koi, H. Sugiyama, M. Ishikawa, T. Inokuchi, N. Shimomura, M. Shimizu, S. Shirotori, B. Altansargai, Y. Ohsawa, K. Ikegami, A. Tiwari, and A. Kurobe

Corporate R&D Center, Toshiba Corporation, Kawasaki 212-8582, Japan

We experimentally demonstrate a giant voltage-control-magnetic-anisotropy (VCMA) coefficient in a crystallographically strained CoFe layer with a relatively thick ferromagnetic CoFe layer (~15 monolayers in thickness) in an MgO/CoFe/Ir system. We observed strong applied voltage dependence on saturation field and asymmetric concave behavior with a giant VCMA coefficient of -758 fJ/Vm and 1043 fJ/Vm. To clarify the mechanism of the observed giant VCMA effect, we investigate the structural and magnetic properties in the MgO/CoFe/Ir system in which giant VCMA was observed. The result reveals epitaxial-like growth in MgO/CoFe/Ir layers and the orientation relationship; MgO (001) [110]// CoFe (001) [100]// Ir (001) [110]. The CoFe layer has a body-centered-cubic (bcc) structure and a tetragonal distortion due to the lattice mismatch. Estimated degree of the lattice distortion (c/a) for bcc CoFe is c/a ~1.09. Since the CoFe layer has the epitaxial strain due to the lattice distortion, the CoFe layer has large

perpendicular magnetic anisotropy. These results suggest that crystallographically strained CoFe system would open a path to realization of low-power-consumption spintronics-based magnetoresistive memories using the giant VCMA effect.

*E-mail address: yushi.kato@toshiba.co.jp

+Present address: Center for Innovative Integrated Electronic Systems, Tohoku University, 468-1 Aramaki-Aza-Aoba, 980-0845 Sendai, Japan

The voltage-control-magnetic-anisotropy (VCMA) effect in magnetic tunnel junctions (MTJs) has been actively investigated with the aim of creating new spintronics-based magnetoresistive memories. Voltage-controlled MTJ (VC-MTJ) was proposed as a low-power nonvolatile memory and it is expected to replace embedded working memories such as static random-access memory (SRAM) [1]. We also recently proposed and demonstrated a voltage-control spintronics memory (VoCSM) employing the VCMA effect as a bit selecting principle and the spin-orbit-torque effect as a writing principle [2-4] for a low-power, high-density nonvolatile memory. Previous studies demonstrated the writing of perpendicular and in-plane MTJs having the VCMA coefficients from 30 to 350 fJ/Vm by applying voltages from a few to several volts. The VCMA coefficients have been experimentally investigated for an ultrathin ferromagnetic layer such as CoFe [5-8], Fe [9-11], FePt [12, 13], FePd [12, 14], CoFeB [15], and FeB [16]. When a voltage is applied to the ultrathin ferromagnetic layer, accumulated charge at the insulator/ferromagnetic metal interface influences the electronic occupation state [17]. As a result, easy axis of the ultrathin ferromagnetic metal layer in MTJs changes owing to the charge accumulation. However, the use of the ultrathin ferromagnetic free layer in MTJs is disadvantageous for observation of a high tunnel magnetoresistance (TMR) ratio. Moreover, the magnitude of VCMA coefficients of 30 - 350 fJ/Vm is insufficient for realizing the high-density memory (VoCSM) we proposed [2-4]. Recently, giant VCMA coefficients of more than 1000 fJ/Vm have been predicted theoretically by *ab initio* calculations in Au/CoFe/MgO and Ta/CoFe/MgO junctions with epitaxially strained CoFe [18-20]. Experimental

demonstrations of the giant VCMA coefficients of 1150 fJ/Vm and 602 fJ/Vm were also reported in MgO/ultrathin-Fe/V [9] and MgO/FePd/Pd [14] systems, respectively. However, ultrathin ferromagnetic free layers (a few monolayers (MLs) in thickness) were also used in these systems for observation of giant VCMA coefficients.

In this paper, we experimentally show a giant VCMA coefficient in a crystallographically strained CoFe layer with a relatively thick ferromagnetic CoFe free layer (~15 MLs in thickness) in an MgO/CoFe/Ir system. We observed a strong applied voltage dependence of saturation field (H_k) and a giant VCMA coefficient reaches more than 1000 fJ/Vm even for the MgO/CoFe/Ir system with a relatively thick ferromagnetic CoFe free layer.

A multilayer stack grown at room temperature on a thermal oxide Si substrate is, from the top surface, Ta (3 nm)/MgO (3 nm)/CoFe (1~3 nm)/Ir (10 nm)/Cr (10 nm)/MgO (3 nm)/CoFeB (2 nm)/Ta (3 nm). The stack was annealed at 300°C for 1 h. To obtain the (001)-oriented Ir and CoFe layers, we used the (001)-template consisting of Cr(001)/MgO(001)/CoFeB/Ta stack. The highly (001)-textured Cr layer and the extremely small roughness were also confirmed by high-resolution scanning transmission electron microscopy (HR-STEM) images. Magnetization measurements were carried out by using a vibrational sample magnetometer (VSM) and the magneto-optical Kerr effect (MOKE). The CoFe free layer has an in-plane magnetization direction. To analyze a radial structure function (RSF), the X-ray absorption fine structure (XAFS) measurement using an X-ray beam line in the SPring-8 synchrotron radiation facility

was used. An XAFS spectrum of standard Fe foil sample was also used in the SPring-8 BL14B2 XAFS database. The stack was patterned and etched by using the photolithograph and Ar ion beam etching (IBE) into device elements 3 × 3 μm^2 to 10 × 10 μm^2 in size. A schematic diagram of the device used in micro-Kerr measurements is shown in Fig. 1(a). The voltage across the multilayer stack, V_{MTJ}, was applied as shown in Fig. 1(a) for observing the perpendicular magnetic anisotropy H_{k_eff} change in the CoFe free layer due to the VCMA effect.

Figure 1(b) shows typical Kerr loops measured under V_{MTJ} = +0.4 V and +1.0 V, and Figure 1(c) shows a typical example of H_{k_eff} measured by using the micro-Kerr effect method as a function of applied voltage for the 5 × 5 μm^2 device. The measured H_{k_eff} exhibited a strong applied voltage dependence. Figure 1(d) shows a typical example of the estimated $K_{u\_eff} \times t_{\_mag}$ as a function of applied electric field E for the 5 × 5 μm^2 device, where K_{u_eff} is the effective magnetic anisotropy energy derived from measured H_{k_eff} and $t_{\_mag}$ is the CoFe thickness. The measured resistance and H_{k_eff} were reproducibly observed, and thus we confirmed that a measurement error of the VCMA coefficient was within 5%. The plots of $K_{u\_eff} \times t_{\_mag}$ versus E had an asymmetric concave shape as shown in Fig. 1(d), and we experimentally observed a giant VCMA coefficient in the MgO/CoFe/Ir system. The magnitude of VCMA coefficients is 1043 fJ/Vm and -758 fJ/Vm. Those values are obtained by estimating the degrees of the inclination of ($K_{u\_eff} \times t_{\_mag}$) vs E plot in Fig. 1(d). Figure 1(e) shows a summary of the VCMA coefficients (dK_S/dE) for the devices fabricated with various junction resistances (sizes). The VCMA coefficients were almost constant

with device size. The average values of the VCMA coefficients are around 1000 fJ/Vm and -300 fJ/Vm in the MgO/CoFe/Ir system. Although some variations of VCMA coefficients from device to device are observed as shown in Fig. 1(e), all devices certainly have giant VCMA effects. To clarify the mechanism of the observed giant VCMA effect, we investigated the detailed structural and magnetic properties as shown below.

Figure 2 shows RSFs around (a) Fe and (b) Co atoms in the CoFe layer. To examine the influence of CoFe thickness on the lattice structures, the XAFS analysis was performed on $Co_{50}Fe_{50}$ (3 nm)/Ir and $Co_{50}Fe_{50}$ (2 nm)/Ir samples. For the reference, data for the $Co_{30}Fe_{70}$ (10 nm) film and Fe-foil having a known bcc-structure and data for Co (12 nm) film with a known face-centered-cubic (fcc)-structure are also plotted in Fig. 2. To obtain the RSFs, the XAFS spectra were Fourier transformed with the photoelectron wave number (k) weight of 3 in k-range of 3~11.7 $Å^{-1}$ for Fig. 2(a) and 3~10.5 $Å^{-1}$ for Fig. 2(b), respectively. In the case of Fe atoms shown in Fig. 2(a), the RSFs for $Co_{50}Fe_{50}$ (2, 3 nm)/Ir are consistent with those for the bcc-structure reference samples ($Co_{30}Fe_{70}$ (10 nm) film and Fe-foil) around 1^{st}, 3^{rd}, and 4^{th} coordination numbers. In the case of Co atoms, as shown in Fig. 2(b), the RSFs for $Co_{50}Fe_{50}$ (2, 3 nm)/Ir are also consistent with those for the bcc-structure reference samples and obviously different from the fcc-structure reference spectrum of Co (12 nm) film. These results indicate that the CoFe layer on Ir underlayer used here has a bcc-structure. From the viewpoint of thickness dependence, the magnitude of the peak intensities for the various coordination numbers has the relation of CoFe (2

nm)/Ir < CoFe (3 nm)/Ir < CoFe (10 nm) < Fe-foil. In the previous study using the CoFe/Pd stacks [21], a change in the structure from tetragonal distortion to the bcc-like structure with increasing CoFe thickness was observed. Our results also indicate that the bcc structure is stabilized with increase in CoFe thickness.

Figure 3 shows (a) cross-sectional HR-STEM image of the typical multilayer stack, together with the fast Fourier transform (FFT) patterns of (b) MgO, (c) CoFe, (d) Ir, and (e) Cr layers. The HR-STEM image shows epitaxial-like growth with crystal grain boundary for MgO/CoFe/Ir/Cr. The FFT patterns of the Cr layer and Ir layer reveal a bcc-structure along the (002) orientation and an fcc structure along the (002) orientation, respectively. The CoFe layer has a bcc-structure with (002) orientation. The MgO layer reveals an fcc (NaCl-type)-structure along the (002) orientation. Therefore, the FFT patterns reveal the orientation relationship of MgO (001)[110]// CoFe (001)[100]// Ir (001)[110]// Cr(001)[100]. Referring to the bulk data, the expected lattice mismatches of MgO/CoFe and CoFe/Ir are 5.0% and 4.5%, respectively. On the other hand, the observed lattice mismatches of MgO/CoFe and CoFe/Ir were 4.5% and 3.7%, respectively. Compared with the bulk data, the lattice constants were close to each other, and thus each layer has an epitaxial strain in the film. According to the FFT analysis, the tetragonal distortion of the CoFe lattice originating from lattice mismatch defined as a c/a is ~1.09, where a and c are lattice constants of a-axis and c-axis. The values of a and c are reduced (-5.96%) and expanded (+2.46%), respectively. In the case of the Cr underlayer (i.e., CoFe/Cr), the tetragonal distortion of the CoFe lattice was also observed and the value is c/a~1.04; shrink of a-axis and expansion of c-axis were -3.16% and

+1.05%, respectively (not shown here). In a previous study, the magnetic anisotropy and crystal structure of tetragonally distorted CoFe with relatively thin thickness (up to 10 MLs) have been investigated. These CoFe thin films show large magnetic anisotropy with c/a~1.13 to 1.24, although these CoFe films have distorted fcc-structure [21, 22]. The quantitative induced strain to the CoFe lattice is related to the lattice mismatch as discussed below (Fig. 4 (a)). Additionally, the result of EDX mapping reveals that any diffusion of Ir elements to the CoFe layer was not detected (not shown here). This result is consistent with the result of the XAFS measurement shown in Fig. 2. The (001) oriented bcc-structure of the CoFe layer on Ir underlayer is suitable for observing large TMR, because the bcc CoFe (001)/MgO (001)/ bcc CoFe (001) hetero-structure exhibits the coherent tunneling effect [23]. In the present work, the prepared stacks have epitaxial-like growth film with many crystal grain boundaries. This indicates that the variations in the strain, orientation, thickness (roughness), and grain boundary size would have an effect on the variation in the VCMA coefficient. For practical memory applications, we need to control the degree of the strain and the orientation of the CoFe lattice more strictly.

Next, we examine the influence of the strain effect on the magnetic properties, such as magnetic dead layer (DL), saturation magnetization (M_S), and perpendicular magnetic anisotropy, for a Ta/MgO/CoFe /underlayers/Cr/MgO/CoFeB/Ta system having the different lattice mismatch between CoFe and underlayer under the condition below the critical CoFe thickness. Figure 4(a) shows critical thickness versus absolute value of lattice mismatch between the CoFe and various underlayers calculated by the

People-Bean equation [24]. In the People-Bean equation, we used the values of 0.3 and 0.4 nm for the Poisson ratio and slip distance, respectively. Below the critical thickness, we expect the preparation of epitaxial strained film to be successful. On the other hand, above the critical thickness, the lattice relaxation takes place. In the case of the Ir under layer, estimated critical thickness is 5 nm. Hereafter, we mainly focus on the case of the Ir under layer, because we observed giant VCMA efficiency in the system with the Ir underlayer. M_S and DL estimated by $M_S \times t$ as a function of CoFe thickness (t) in the range of 1.5 to 10 nm are shown in Fig. 4(b). The plot shows excellent linearity, allowing accurate estimations of the DL and M_S values in the CoFe layer. The error bars of the CoFe thickness shown in Fig. 4(b) are mainly due to the film roughness. The estimated M_S and DL for the CoFe layer on the Ir underlayer are 1950 emu/cm^3 and 0.5 nm, respectively.

Figures 4(c) and 4(d) show H_{k_eff} and K_{u_int} of the CoFe layer plotted against the CoFe thickness for the Ir and Cr underlayers. The magnitude of negative H_{k_eff} values indicates the existence of in-plane magnetic anisotropy in the CoFe layer. The estimated interface magnetic anisotropy K_S of MgO/CoFe/Ir was 1.91 erg/cm^2. In the case of the Cr underlayer, the H_{k_eff} and the K_{u_int} values were almost constant with increasing CoFe thickness in the range less than 3 nm. In this range of the CoFe thickness (1~3 nm), at least, these data indicate that the CoFe layer film has strain without any lattice relaxation. On the other hand, in the case of the Ir underlayer, the lattice relaxation of the CoFe layer was observed at around 1.2 nm thickness as shown in Figs. 4(c) and 4(d). The perpendicular magnetic anisotropy (H_{k_eff} and K_{u_int}) of

the CoFe layer on the Ir underlayer is larger than in the case of the Cr underlayer as shown in Figs. 4(c) and 4(d). This result indicates that the CoFe layer on the Ir underlayer still has the epitaxial strain in the case of the CoFe thickness of less than 3.0 nm, even though some kind of lattice relaxation is observed in the CoFe layer thickness range between 1.2 nm and 3.0 nm. The perpendicular magnetic anisotropy and the critical thickness of the CoFe layer on the Ir underlayer are larger and smaller than those on the Cr underlayer, respectively. This behavior is consistent with the estimated critical thickness shown and discussed in Fig. 4(a). The properties correspond to the lattice mismatch between CoFe and underlayers (Cr, Ir).

Finally, we discuss the correlation between strain and the VCMA effect. According to first-principles calculation by Burkert et al. [25], the energy separation between the $d_{x^2-y^2}$ and d_{xy} states is reduced by tetragonal distortion. Therefore, the perpendicular magnetic anisotropy of CoFe would be enhanced owing to distortion, because the magnetic anisotropy energy is inversely proportional to the energy separation between the occupied and unoccupied states ($d_{x^2-y^2}$ and d_{xy}) located below and above the Fermi level. In our experiment, the accumulated charge applied by voltage directly influences the electronic occupation state. As a result, the magnetic anisotropy energy responds sensitively to applied voltage. Other theoretical studies [18-20] support our experimental results with respect to the giant VCMA efficiency and asymmetric concave behavior, for example. According to their calculations, the critical field where the magnetic anisotropy reaches its maximum or minimum value depends on the interplay

between the internal and external *E* fields where the internal *E* field can be tuned by strain. However, the origin of the observed giant VCMA effect is as yet unclear. To clarify the mechanism of the giant VCMA effect, theoretical calculation and further systematic investigations, such as the correlation between CoFe thickness, strain, and the VCMA effect, would be necessary in future work.

In summary, we experimentally demonstrated a giant VCMA coefficient in a crystallographically strained CoFe layer with a relatively thick ferromagnetic CoFe layer (~15 MLs in thickness) in an MgO/CoFe/Ir system. The VCMA effect exhibited a strong applied voltage dependence on H_k, and it showed an asymmetric concave behavior with giant VCMA coefficients of 1043 fJ/Vm and -758 fJ/Vm. The structural analysis revealed epitaxial-like growth with the orientation relationship; MgO (001)[110]// CoFe (001)[100]// Ir (001)[110]. The CoFe layer had a bcc-structure and a tetragonal distortion due to the lattice mismatch. We also found that since the CoFe layer has the epitaxial strain, the CoFe layer showed large perpendicular magnetic anisotropy energy. The crystallographically strained CoFe system would open a path to realizing the giant VCMA efficiency required for ultra-low-power-consumption spintronics-based magnetoresistive memories using the VCMA effect.

Acknowledgements

This work was partly supported by the ImPACT Program of the Council for Science, Technology and Innovation (Cabinet Office, Government of Japan). The synchrotron radiation experiments were

performed at the BL16B2 of SPring-8 with the approval of the Japan Synchrotron Radiation Research Institute (JASRI) (Proposal No. 2012A5360 and 2017A5360).

REFERENCES

[1] K. Ikegami, Y. Shiota, T. Nozaki, K. Abe, H. Noguchi, S. Yuasa, Y. Suzuki, and S. Fujita, in Intermag Digest (2017), CF-11.

[2] H. Yoda, N. Shimomura, Y. Ohsawa, S. Shirotori, Y. Kato, T. Inokuchi, Y. Kamiguchi, B. Altansargai, Y. Saito, K. Koi *et al.*, in IEDM Technical Digest (2016), p. 27-6.

[3] T. Inokuchi, H. Yoda, Y. Kato, M. Shimizu, S. Shirotori, N. Shimomura, K. Koi, Y. Kamiguchi, H. Sugiyama, S. Oikawa *et al.*, Appl. Phys. Lett. **110**, 252404 (2017).

[4] S. Shirotori, H. Yoda, Y. Ohsawa, N. Shimomura, T. Inokuchi, Y. Kato, Y. Kamiguchi, K. Koi, K. Ikegami, H. Sugiyama *et al.*, IEEE Trans. Magn., **53**, 3401104 (2017).

[5] T. Nozaki, Y. Shiota, M. Shiraishi, T. Shinjo, and Y. Suzuki, Appl. Phys. Lett. **96**, 022506 (2010).

[6] Y. Shiota, T. Maruyama, T. Nozaki, T. Shinjo, M. Shiraishi, and Y. Suzuki, Appl. Phys. Express **2**, 063001 (2009).

[7] T. Nozaki, Y. Shiota, S. Murakami, F. Bonell, S. Ishibashi, H. Kubota, K. Yakushiji, T. Saruya, A. Fukushima, S. Yuasa, T. Shinjo, and Y. Suzuki, Nat. Phys. **8**, 491 (2012).

[8] Y. Shiota, T. Nozaki, F. Bonell, S. Murakami, T. Shinjo, and Y. Suzuki, Nat. Mater. **11**, 39 (2012).

[9] A. Rajanikanth, T. Hauet, F. Montaigne, S. Mangin, and S. Andrieu, Appl. Phys. Lett. **103**, 062402 (2013).

[10] T. Nozaki, A. K. –Rachwal, W. Skowroński, V. Zayets, Y. Shiota, S. Tamaru, H. Kubota, A.

Fukushima, S. Yuasa, and Y. Suzuki, Phys. Rev. Appl. **5**, 044006 (2016).

[11] T. Maruyama, Y. Shiota, T. Nozaki, K. Ohta, N. Toda, M. Mizuguchi, A. A. Turapurkar, T. Shinjo, M. Shiraishi, S. Mizukami, Y. Ando, and Y. Suzuki, Nat. Nanotechnol. **4**, 158 (2009).

[12] M. Weisheit, S. Fähler, A. Marty, Y. Souche, C. Poinsignon, and D. Givord, Science **315**, 349 (2007).

[13] T. Seki, M. Kohda, J. Nitta, and K. Takanashi, Appl. Phys. Lett. **98**, 212505 (2011).

[14] F. Bonell, S. Murakami, Y. Shiota, T. Nozaki, T. Shinjo, and Y. Suzuki, Appl. Phys. Lett**. 98**, 232510 (2011).

[15] M. Endo, S. Kanai, S. Ikeda, F. Matsukura, and H. Ohno, Appl. Phys. Lett. **96**, 212503 (2010).

[16] T. Nozaki, K. Yakushiji, S. Tamaru, M. Sekine, R. Matsumoto, M. Konoto, H. Kubota, A. Fukushima, and S. Yuasa, Appl. Phys. Express 6, 073005 (2013).

[17] P. Bruno, Phys. Rev. B, **39**, 865 (1989).

[18] D. Odkhuu, Sci. Rep. **6**, 32742 (2016).

[19] P. V. Ong, N. Kioussis, P. K. Amiri, and K. L. Wang, Sci. Rep. **6**, 29815 (2016).

[20] P. V. Ong, N. Kioussis, D. Odkhuu, P. K. Amiri, K. L. Wang, and G. P. Carman, Phys. Rev. B **92**, 020407(R) (2015).

[21] A. Winkelmann, M. Przybylski, F. Luo, Y. Shi, and J. Barthel, Phys. Rev. Lett. **96**, 257205 (2006).

[22] F. Luo, X. L. Fu, A. Winkelmann, and M. Przybylski, Appl. Phys. Lett. **91**, 262512 (2007).

[23] W. H. Butler, X. –G. Zhang, and T. C. Schulthess, Phys. Rev. B. **63**, 054416 (2001).

[24] R. People and J. C. Bean, Appl. Phys. Lett. **47**, 322 (1985).

[25] T. Burkert, L. Nordström, O. Eriksson, and O. Heinonen, Phys. Rev. Lett. **93**, 027203 (2004).

Figure Captions

Fig. 1 (a) Schematic diagram of the device used in micro-Kerr measurements, (b) representative Kerr loops measured under V_{MTJ} = +0.4 V and +1.0 V, (c) typical example of measured H_{k_eff} versus applied voltage, (d) typical example of estimated $K_{u\_eff} \times t_{\_mag}$ as a function of applied electric field E, and (e) summary of the VCMA effect (dK_S/dE) versus resistance of the fabricated devices.

Fig. 2 RSFs (radial structure functions) around (a) Fe and (b) Co atoms in the CoFe layers.

Fig. 3 (a) Cross-sectional high-resolution scanning transmission electron microscopy (HR-STEM) image of the typical multilayer stack, and Fourier transform patterns of (b) MgO, (c) CoFe, (d) Ir, and (e) Cr layers.

Fig. 4 (a) Critical thickness versus absolute value of lattice mismatch between the CoFe and various underlayers calculated by People-Bean equation. (b) M_S and DL estimated by $M_S t$ as a function of CoFe thickness. (c) H_{k_eff} and (d) K_{u_int} of the CoFe layer plotted against the CoFe thickness for Ir and Cr underlayers.

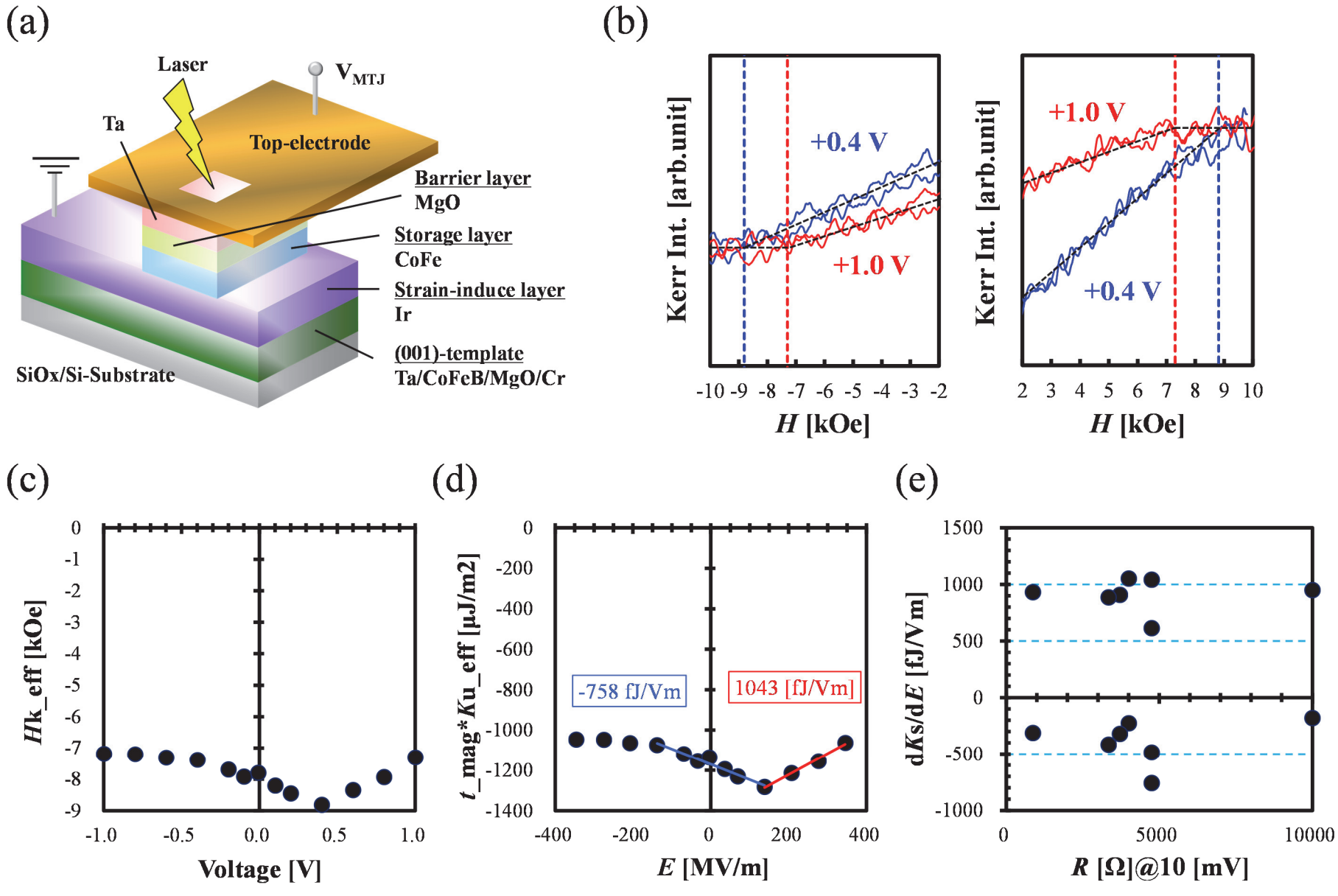
(a)
Laser
V_{MTJ}
Ta
Top-electrode
Barrier layer
MgO
Storage layer
CoFe
Strain-induce layer
Ir
(001)-template
Ta/CoFeB/MgO/Cr
SiOx/Si-Substrate
(b)
Kerr Int. [arb.unit]
+0.4 V
+1.0 V
H [kOe]
+1.0 V
+0.4 V
Kerr Int. [arb.unit]
H [kOe]
(c)
Hk_eff [kOe]
Voltage [V]
(d)
t_mag*Ku_eff [μJ/m2]
-758 fJ/Vm
1043 [fJ/Vm]
E [MV/m]
(e)
dKs/dE [fJ/Vm]
R [Ω]@10 [mV]

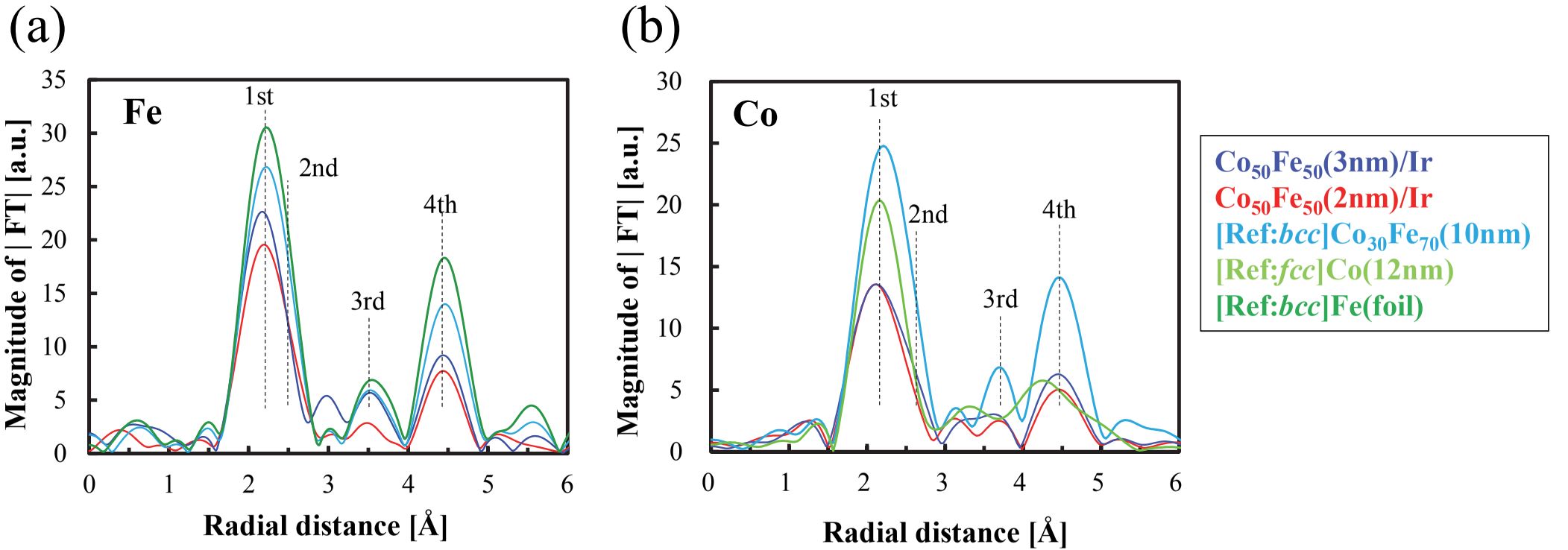
(a)
Fe
1st
2nd
3rd
4th
Magnitude of | FT| [a.u.]
Radial distance [Å]
(b)
Co
1st
2nd
3rd
4th
Magnitude of | FT| [a.u.]
Radial distance [Å]
Co50Fe50(3nm)/Ir
Co50Fe50(2nm)/Ir
[Ref:bcc]Co30Fe70(10nm)
[Ref:fcc]Co(12nm)
[Ref:bcc]Fe(foil)

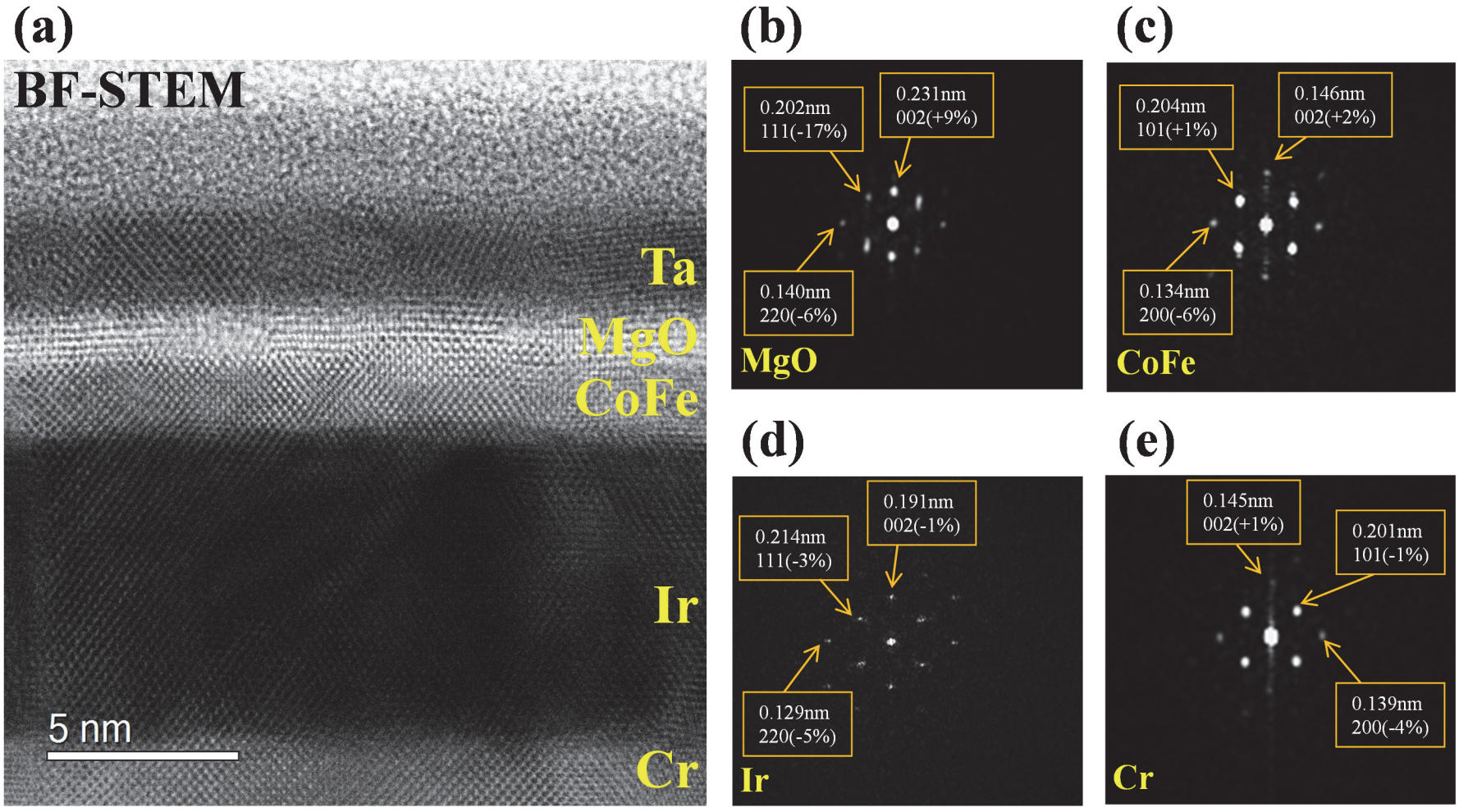
(a)
BF-STEM
Ta
MgO
CoFe
Ir
Cr
5 nm
(b)
0.202nm
111(-17%)
0.231nm
002(+9%)
0.140nm
220(-6%)
MgO
(c)
0.204nm
101(+1%)
0.146nm
002(+2%)
0.134nm
200(-6%)
CoFe
(d)
0.214nm
111(-3%)
0.191nm
002(-1%)
0.129nm
220(-5%)
Ir
(e)
0.145nm
002(+1%)
0.201nm
101(-1%)
0.139nm
200(-4%)
Cr

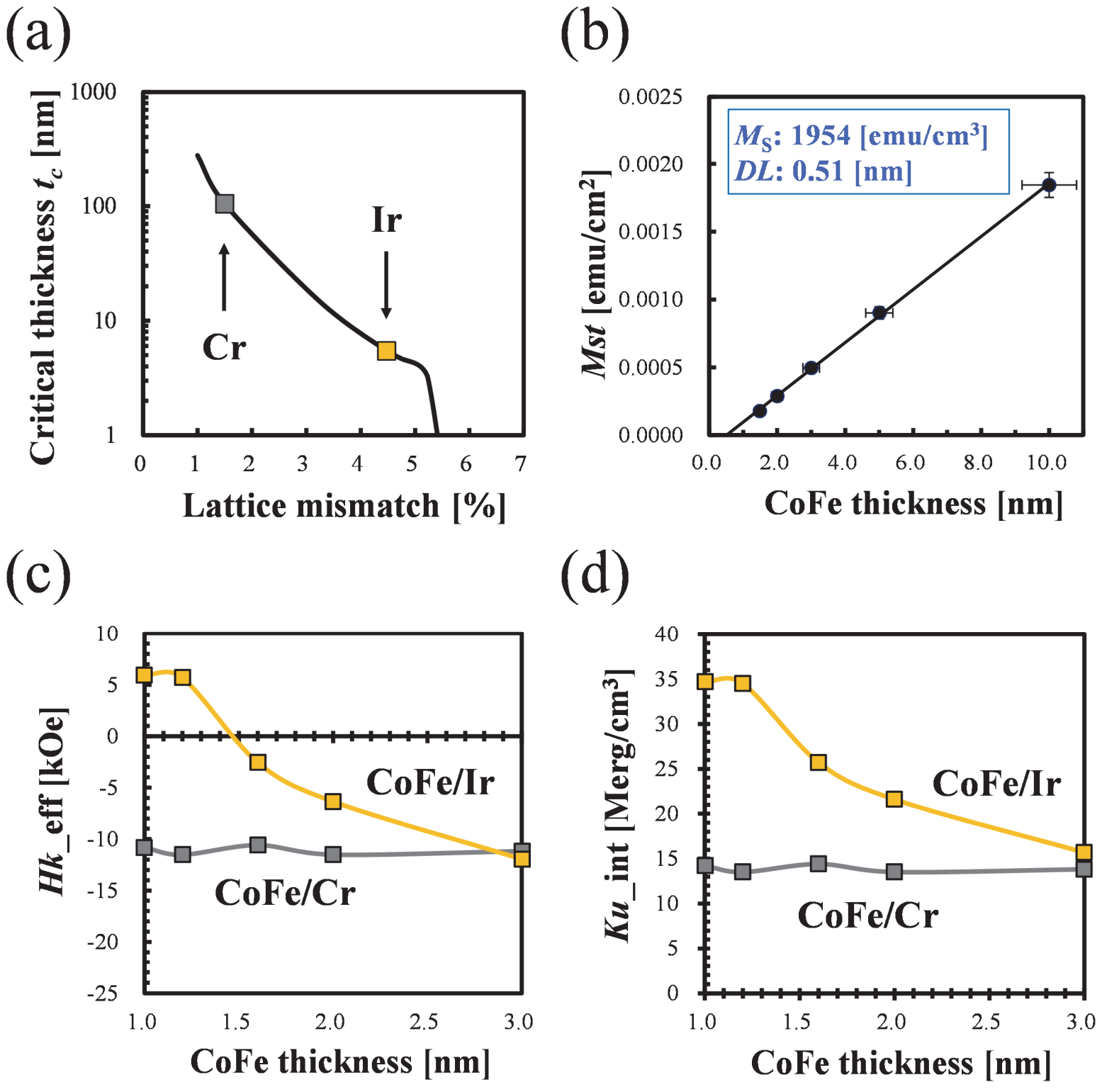
(a)
Critical thickness t_c [nm]
1000
100
10
1
0
1
2
3
4
5
6
7
Lattice mismatch [%]
Cr
Ir
(b)
M_S: 1954 [emu/cm^3]
DL: 0.51 [nm]
Mst [emu/cm^2]
0.0025
0.0020
0.0015
0.0010
0.0005
0.0000
0.0
2.0
4.0
6.0
8.0
10.0
CoFe thickness [nm]
(c)
Hk_eff [kOe]
10
5
0
-5
-10
-15
-20
-25
1.0
1.5
2.0
2.5
3.0
CoFe thickness [nm]
CoFe/Ir
CoFe/Cr
(d)
Ku_int [Merg/cm^3]
40
35
30
25
20
15
10
5
0
1.0
1.5
2.0
2.5
3.0
CoFe thickness [nm]
CoFe/Ir
CoFe/Cr